RESEARCH ARTICLE

Macromolecular Rapid Communications
www.mrc-journal.de

Mimicking Enzymatic Non-Covalent Interactions with Functionalized Covalent Organic Frameworks for Improved Adsorption and Hydrolysis of Cellobiose

*Pui Ching Lan, Yin Zhang, Weijie Zhang, Xueying Ge, and Shengqian Ma**

Tuning catalytic centers in heterogeneous catalyst, both in a chemical and a spatial manner, is a powerful approach to improve the stability and the efficiency of catalysts. While the chemical aspects are largely understood, the spatial interactions around active sites, comprised of non-covalent interactions, are difficult to maintain and challenging to study. Herein, the unique properties of covalent organic frameworks (COFs) are utilized to establish an ideal reaction environment for the hydrolysis of cellobiose and other common disaccharides in mild, metal-free, and neutral aqueous conditions. The chosen COF, HCl-PSA-IM-COF-OMe ("HCl" for hydrochloric acid, "PSA" for propyl sulfonic acid, "IM" for imidazole, and "OMe" for methoxy), is modified to be ultra-stable in aqueous conditions and possesses sulfonic acid groups for general acid catalysis and for enhanced hydrogen bonding with reactants as well as intraporous chloride anions for oxocarbenium intermediate stabilization. In addition, the system also relies on the differences in adsorptive binding behavior, K_{ads}, of the reactants and the products to the functionalized framework and benefits from a separate physical, kinetic process to boost the catalytic cycle. Due to its stability in aqueous conditions, HCl-PSA-IM-COF-OMe can be recycled and maintains its hydrolytic properties for five cycles before regeneration is needed.

1. Introduction

In heterogeneous catalysis, the ability to attract reactants to catalytic centers is often directly linked to the catalyst's activities, both in terms of longevity and efficiency.[1] To establish this attraction, catalysts, especially enzymes, were strategically designed to accommodate specific non-covalent interactions, leading to selectivity and stabilization of transition state.[2] Unlike homogeneous catalysts, there are more challenges to overcome for heterogeneous systems, such as catalytically active surface area,[3] mass transport,[4] and compatibilities of support materials in various chemical conditions.[3a,5] It is thus of great interest to design a heterogeneous catalyst that incorporates the quintessential features of homogeneous catalysts while mitigating the traditional difficulties faced by heterogeneous catalysts.

To illustrate, the hydrolysis of cellobiose, as well as other common disaccharides, in water was chosen as the model reaction. The glycosidic bond (equivalent to acetal group) is one of the most resilient, naturally occurring linkage between two or more saccharide molecules, requiring up to 150 kJ mol^{-1} of activation energy to hydrolyze the bond in acidic aqueous condition.[6] Due to its inertness, it is utilized as protecting group for ketones and aldehydes in a variety of synthetic conditions. However, it is also this inertness that prevents access to Earth's most abundant carbon sources—cellulose. Cellulose is a biopolymer, made up of glucose molecules arranged in a linear fashion. The spatial arrangements of hydroxy groups allow for intermolecular hydrogen bonding between each chain, forming not only a stable, but also a crystalline structure. These glucose molecules, hidden away in an array of complex hydrogen bonding network and chemically protected by glycosidic bonds, are believed to be the solution to not only a sustainable source of clean energy but also a diversified energy supplies, leading to long term energy security.[7] The current direction of climate change initiatives promote clean energy, thus fossil fuel alternatives that produce similar emissions to gasoline overall are no longer adequate. Glucose can be fermented to bioethanol, which contains roughly 70% of the energy equivalent to gasoline but burns much cleaner.[8] Along with other glucose-derived fuels, such as 2,5-dimethylfuran and methylfuran (both of which pack a comparable energy density, blending abilities, and relatively high octane numbers to gasoline),[9] combustion of bioethanol can be made into an overall carbon-neutral process. It is this clean combustion aspect of bioethanol that currently makes it the clear favorite as gasoline alternative, however, efficient hydrolysis of glycosidic bonds remains a challenging chemistry problem, even through years of genetic evolution and selection.

Glycoside hydrolase, such as cellobiase and cellulase, can promote specific binding with disaccharides through numerous spatial arrangements of favorable non-covalent interactions.[10] Such arrangement isolates all reactive parties, in particular acidic protons,[3a,11] glycosidic bonds, and nucleophilic water, into a

P. C. Lan, Y. Zhang, W. Zhang, X. Ge, S. Ma
Department of Chemistry
University of North Texas
Denton, TX 76210, USA
E-mail: Shengqian.Ma@unt.edu

The ORCID identification number(s) for the author(s) of this article can be found under https://doi.org/10.1002/marc.202200724

DOI: 10.1002/marc.202200724

reaction environment that increases acidity and nucleophilicity of molecules that normally are not considered acidic nor nucleophilic,[12] thus decreasing activation energy (5–50 kJ mol^{-1} for glycoside hydrolase, depending on species, pH, temperature, and solvent).[13] To achieve this isolation, two main interactions are utilized in enzymes—hydrogen bonding and stacking or hydrophobic interaction. Hydrogen bonding occurs between the polar amino acid residues and the hydroxy groups of saccharides, up to three bonds per saccharide (one as donor and two as acceptor). Despite being one of the strongest non-covalent interactions, hydrogen bonding is not the primary interaction for saccharide recognition in enzyme. When examining the structure of a cellobiose molecule, there exist two distinct electronic regions. The polar hydroxy groups populate the equatorial positions, creating a hydrophilic skirt around the molecule, while the nonpolar C–H bonds occupy the axial positions, creating hydrophobic regions above and below the molecule. Glucosidase, such as Bgl3A found in fungi, has an unusually hydrophobic binding pocket for cellobiose that have hydrophobic residues strategically arranged to interact with the cellobiose's hydrophobic regions above and below the molecule while minimum amounts of hydrophilic residues exist to serve as catalytic components. Stacking or hydrophobic interaction occurs between the aromatic residues and the axial C–H bonds of cellobioses.[14] There are three driving forces behind this stacking interaction: 1) the partial negative aromatic ring and the partial positive C–H bond form an electrostatic interaction, 2) in conjunction with London dispersion forces, and 3) the favorable effect from solvation and desolvation processes.[15] Both these interactions, while opposites in terms of polarities, work synergistically to promote recognitions and to strengthen saccharide–enzyme complexes. To capture some of these unique chemical interactions, a variety of porous materials have been developed to house the delicate enzymes, which only function at very specific chemical conditions. Porous materials aimed to protect enzymes from harsh conditions while providing a stable condition to maintain their catalytic cycles.[16] However, a combination of enzyme leakage, forced conformational changes, and limited mass transfer prevented enzyme encapsulation systems from gaining traction in practical applications. Instead, it may be more purposeful to replicate enzymatic non-covalent interactions in heterogeneous catalysts using a crystalline material with predictable arrangements serving as the basic scaffold with the flexibility to decorate a variety of functional groups to build the ideal reaction environment.

Covalent organic frameworks (COFs) is a class of crystalline porous material constructed entirely from organic building blocks.[17] The geometric construction creates periodic, ordered pores which gift them internal surface area and internal volume, making them excellent host materials for guest molecules.[18] Due to its organic nature, the pore surface is also susceptible to typical chemical transformations, allowing for installation of myriads of functional groups.[19] Both aspects can be utilized to strategically organize an active site that chemically and spatially supports full catalytic cycles, from creating a desirable solvation environment[1a] to binding of reactants to initiation to transition state stabilization to product release. To accomplish this in COF, several functional groups were installed in its weakly hydrophilic pores to replicate some of the saccharide binding interactions found in glycoside hydrolases.

2. Results and Discussion

2.1. Material Preparation and Characterization

TAPB-DMTP-COF (denoted as COF-OMe hereafter, "OMe" for methoxy groups), synthesized by the condensation between 1,3,5-tris(4-aminophenyl)benzene (TAPB) and 2,5-dimethoxyterephthaldehyde (DMTP), was chosen as the fundamental porous framework for this experiment (modification scheme shown in **Figure 1**).[18a,18d] Despite its incredible stability in various organic solvents,[20] the imine linkage is susceptible to nucleophilic attack by water in the presence of acid, both of which are essential components for the hydrolysis of glycosidic bonds. To improve the stability of COF-OMe in aqueous conditions, the aromatic imine linkage was modified by cycloaddition of 1-vinylimidazole in the presence of ytterbium (III) triflate and aromatization by 2,3-dichloro-5,6-dicyano-*p*-benzoquinone (DDQ) to form the ultra-stable quinoline-linked COF (denoted as IM-COF-OMe, "IM" for imidazole), a method (the Povarov reaction) first pioneered by Liu et al in 2018 with styrene and then expanded to 1-vinylimidazole by Dong et al in 2021.[21] Subsequent nucleophilic attack by the imidazole group to the electrophilic 1,3-propane sultone and protonation with hydrochloric acid[21b] produced a COFs with both ionic and Brønsted acid moieties (denoted as HCl-PSA-IM-COF-OMe, "PSA" for propyl sulfonic acid), which Dong et al used as a heterogeneous Brønsted acid catalyst for the Biginelli reaction.

To confirm the successful integration of new functional groups, X-ray photoelectron spectroscopy (XPS), Fourier transform infrared spectroscopy (FTIR), ^{13}C and ^{31}P solid state nuclear magnetic resonance spectroscopy (NMR), and elemental analysis were performed. As shown in Figure S3, Supporting Information, the two signals of S $2p_{3/2}$ (at ≈165 eV) and S $2p_{1/2}$ (at ≈166 eV) confirmed the presence of sulfur in HCl-PSA-IM-COF-OMe, and, along with a signal for S=O (at ≈529 eV from O 1s), confirmed the presence of sulfonic acid groups ($-SO_3H$). A distinct peak at ≈286 eV from C 1s and at ≈399 eV from N 1s were good indicators of imidazolium groups. Last, two signals of Cl $2p_{3/2}$ (at ≈198 eV) and $2p_{1/2}$ (at ≈200 eV) corresponded well with chloride anions. FTIR analysis (Figure S1, Supporting Information) further supported the integration of these functional groups. The aromatization of imine bond with 1-vinylimidazole was verified with the emergence of quinolyl group at ≈1550 cm^{-1}.[21d,22] The evidence of successful propyl sulfonic acid functionalization was indicated by the emergence of iminium ($C{=}N^+R_2$) peak at ≈1647 cm^{-1} and the decrease in intensity of the imine (C=N) bond at 1589 cm^{-1}.[21a] Peaks associated with propyl sulfonic acid group were ≈1213 cm^{-1} (S=O asymmetric stretch overlapping with Ar C–N stretch), ≈1169 cm^{-1} (S=O symmetric stretch), ≈1032 cm^{-1} (S–O stretch overlapping with Alkyl C-O stretch), and ≈608 cm^{-1} (C–S stretch). Elemental analysis indicated a sulfur content of 3.56 wt% and stoichiometric calculation from back titration with aqueous sodium chloride and aqueous sodium hydroxide showed a sulfonic acid content of 0.92 mmol $-SO_3H$ per gram COF (Tables S1 and S2, Supporting Information). The relative acidity was determined using 4-nitroaniline (pK_a of conjugate acid = 0.99 in water) as probe molecule and ultraviolet–visible (UV–vis) spectroscopy. Using Equation (2), the Hammett acidity function, H_0, of

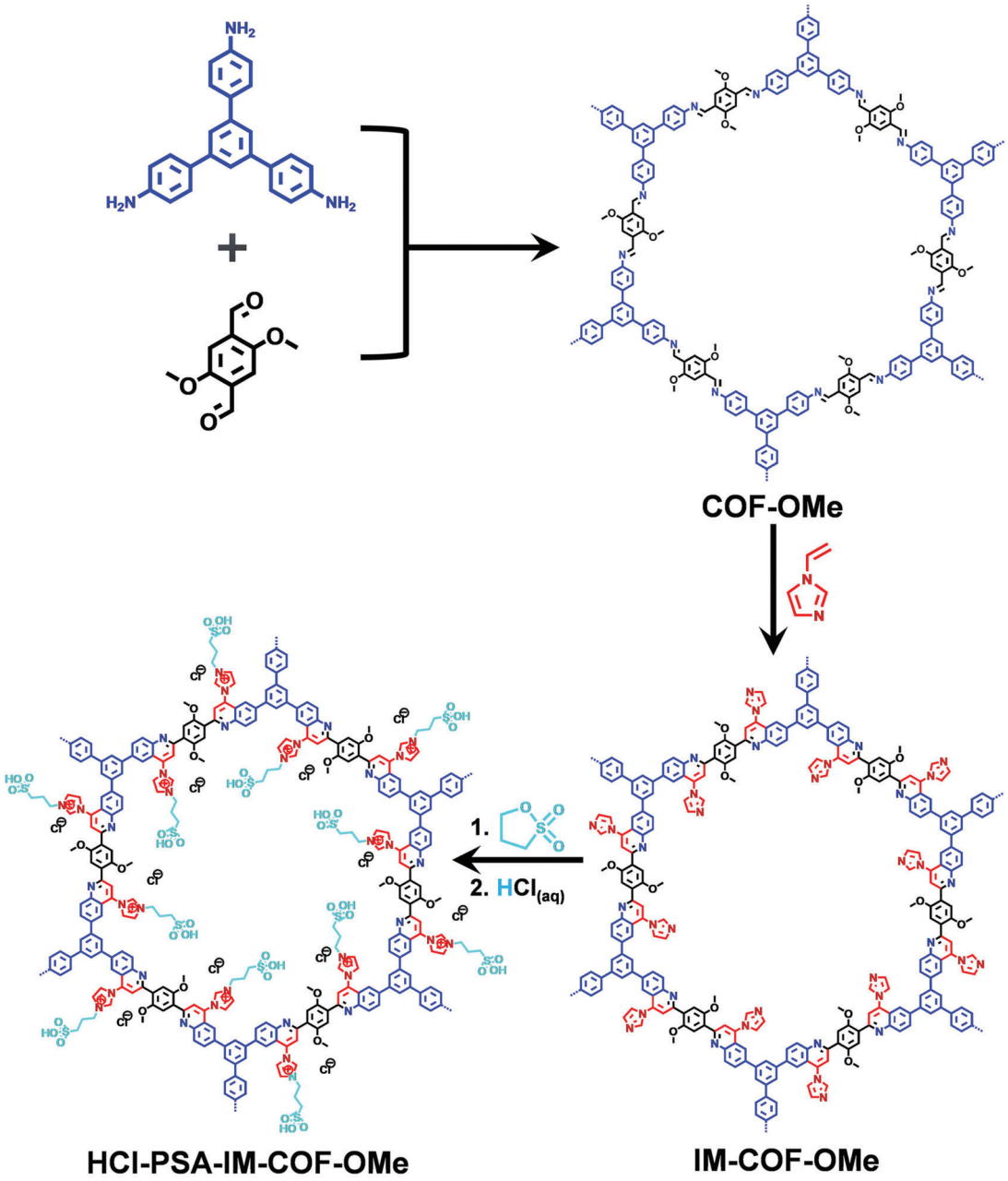

Figure 1. The schematic for the construction of HCl-PSA-IM-COF-OMe, a covalent organic framework featuring ionic moiety, strong Brønsted acid, and ultra-stable quinoline linkages.

HCl-PSA-IM-COF-OMe was calculated to be 1.64, which is comparable in acidity to 3-hydroxypropanesulfonic acid$_{(aq)}$ (H_0 = 1.50), sulfuric acid$_{(aq)}$ (H_0 = 1.44), and *p*-toluenesulfonic acid$_{(aq)}$ (H_0 = 1.61) (Table S3, Supporting Information). Another method to evaluate the acid strength of this solid porous acid is the use of trimethylphosphine oxide (TMPO). A known quantity of TMPO was adsorbed to the framework and the solid state ^{31}P NMR spectroscopy was performed using diammonium hydrogen phosphate as internal standard (ppm = 1.0). The resulting spectrum (Figure S10, Supporting Information) showed two board peaks—one at ≈45.2 ppm, which corresponds to TMPO adsorbed to the framework, and another at ≈77.9 ppm, which corresponds to TMPO's interaction to a Brønsted acid site, polarizing the phosphorus–oxygen bond. At ≈77.9 ppm chemical shift, it indicates strong to very strong acidity.[23]

Seeing that the sulfonic acid groups were successfully grafted, further structural characterizations were performed. As shown in **Figure 2a**, Powder X-ray diffraction (PXRD) patterns for COF-OMe, IM-COF-OMe, and HCl-PSA-IM-COF-OMe verified that the crystalline structures were retained after two sequential chemical modifications. Successful post-synthetic modifications were also evident with decreases in Brunauer–Emmett–Teller

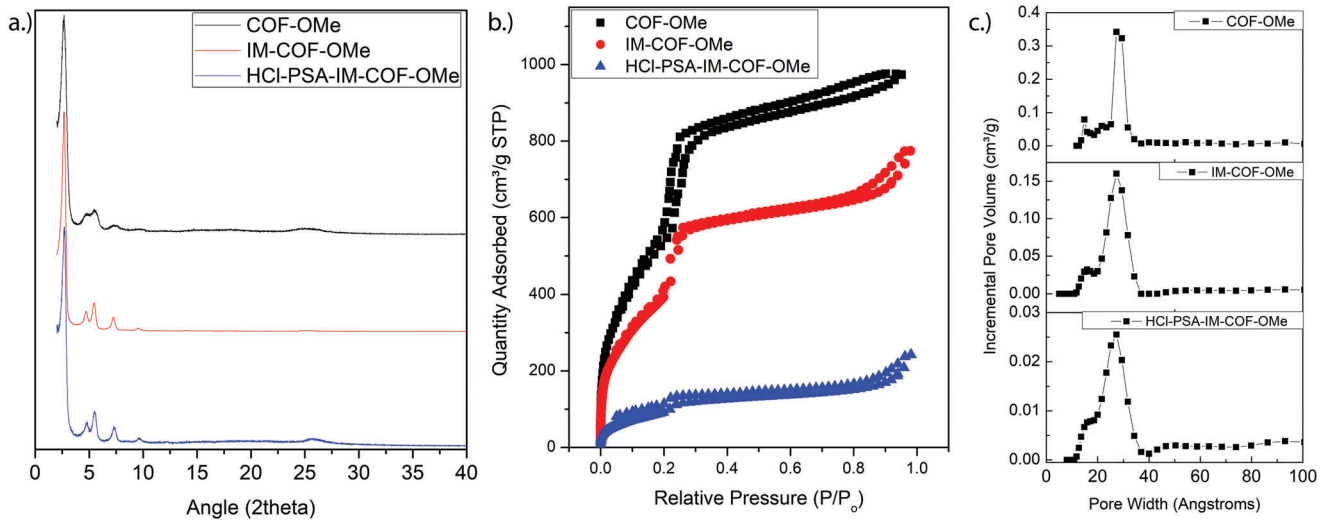

Figure 2. A comparison of a) PXRD patterns, b) N_2 sorption isotherms at 77 K, and c) pore size distributions of COF-OMe, IM-COF-OMe, and HCl-PSA-IM-COF-OMe.

(BET) surface area and pore volumes (Figure 2b,c). Starting with a surface area of 2295 m^2 g^{-1} and a pore volume of 1.347 cm^3 g^{-1} for COF-OMe, the addition of the small 1-vinylimidazole moiety only slightly decreased the surface area and pore volume to 1814 m^2 g^{-1} and 1.201 cm^3 g^{-1}, respectively. The addition of propylsulfonic acid and protonation with hydrochloric acid showed a more dramatic decrease, down to 400 m^2 g^{-1} and 0.376 cm^3 g^{-1}, due to protrusion of propylsulfonic acid group well into the pore space. While the measured pore size distribution of COF-OMe and its derivatives were relatively unchanged, it is worth noting that the frequency of pore width changed due to non-uniformal pore modifications. Thermogravimetric analysis (TGA) showed thermal stability up to 400 °C for COF-OMe and up to 200 °C for IM-COF-OMe and HCl-PSA-IM-COF-OMe (Figure S2, Supporting Information).

Unlike homogeneous reaction, it is necessary for reactants in heterogeneous reaction to exhibit a degree of intermolecular attraction with the surface of the catalyst. Since the solvent for proposed cellobiose hydrolysis is water, the pore surface of HCl-PSA-IM-COF-OMe should ideally be hydrophilic. To determine the hydrophilicity, the water contact angle measurements were obtained. Starting with COF-OMe and IM-COF-OMe, the contact angles were 63.4° and 73.3°, respectively. After functionalization with 1,3-propane sultone, the contact angle became 44.2°, demonstrating an improved hydrophilicity with sulfonic acid groups on the pore surface (Figure S5, Supporting Information). To quantify this interaction, the uptake of cellobiose and glucose were measured. Using the Langmuir's equation (Equation (1)), the theoretical maximum adsorption capacity at 298.15 K for cellobiose and for glucose were determined to be 5 g per gram COF and 2 g per gram COF, respectively, and the calculated binding affinities (K_{ads}) were 6.75 M^{-1} for cellobiose and 25.6 M^{-1} for glucose. The Gibbs free energy (ΔG) for adsorption were calculated from K_{ads} and were determined to be −4.73 kJ mol^{-1} for cellobiose and −8.03 kJ mol^{-1} for glucose at 298.15 K, both of which indicate spontaneous interactions with HCl-PSA-IM-COF-OMe and are neither too strong nor too weak when compared with saccharide–enzyme complexes (ΔG = −32 to −6 kJ mol^{-1}, depending chain length, species, and other physiological factors).[24] Subsequent BET surface area and pore volume measurements indicated decreases in both metrices, from BET of 400 m^2 g^{-1} and pore volume of 0.376 cm^3 g^{-1} for pristine down to 227 m^2 g^{-1} and 0.251 cm^3 g^{-1} for cellobiose and down to 168 m^2 g^{-1} and 0.179 cm^3 g^{-1} for glucose (Figure S7 and Table S4, Supporting Information). As shown by the PXRD patterns, having cellobiose and glucose as guest molecules did not destroy the integrity of the frameworks, indicating purely surface interactions (Figure S8, Supporting Information).

2.2. Cellobiose Hydrolysis

Cellobiose hydrolysis was used as the model reaction to examine the HCl-PSA-IM-COF-OMe's hydrolytic capabilities of glycosidic bonds. In a typical reaction, HCl-PSA-IM-COF-OMe, cellobiose, and deuterium oxide were heated at 100 °C for 24 h. Using quantitative ^{1}HNMR (**Figure 3**), it was calculated that 77.5% of cellobiose were hydrolyzed within that time frame with 2.5% of it converted to the aldehyde derivatives (5-hydroxymethylfurfural, furfural, glyceraldehyde, and glycolaldehyde) and 0.8% to formic acid (**Figure 4**). For comparison, control (with no COF addition), COF-OMe, IM-COF-OMe, 3-hydroxypropanesulfonic $acid_{(aq)}$, a mixture of IM-COF-OMe and 3-hydroxypropanesulfonic acid, and Amberlyst 15 (4.6 mmol $-SO_3H$ g^{-1}, 36 m^2 g^{-1}), yielded 1.8%, 1.1%, 3.3%, 61.1%, 3.5%, and 9.8%, respectively, under the same reaction condition (**Table 1**). The stability of the glycosidic bond is demonstrated with the two control experiments where 1.8% and 1.1% of the cellobiose were hydrolyzed under neutral condition. Interestingly, the addition of basic imidazole groups on IM-COF-OMe slightly increased the percent conversion (up to 3.3%), even with the addition of 3-hydroxypropanesulfonic acid to IM-COF-OMe. Under acidic conditions, it is expected that 3-hydroxypropanesulfonic acid can hydrolyze cellobiose, but surprisingly at a percentage lower than HCl-PSA-IM-COF-OMe.

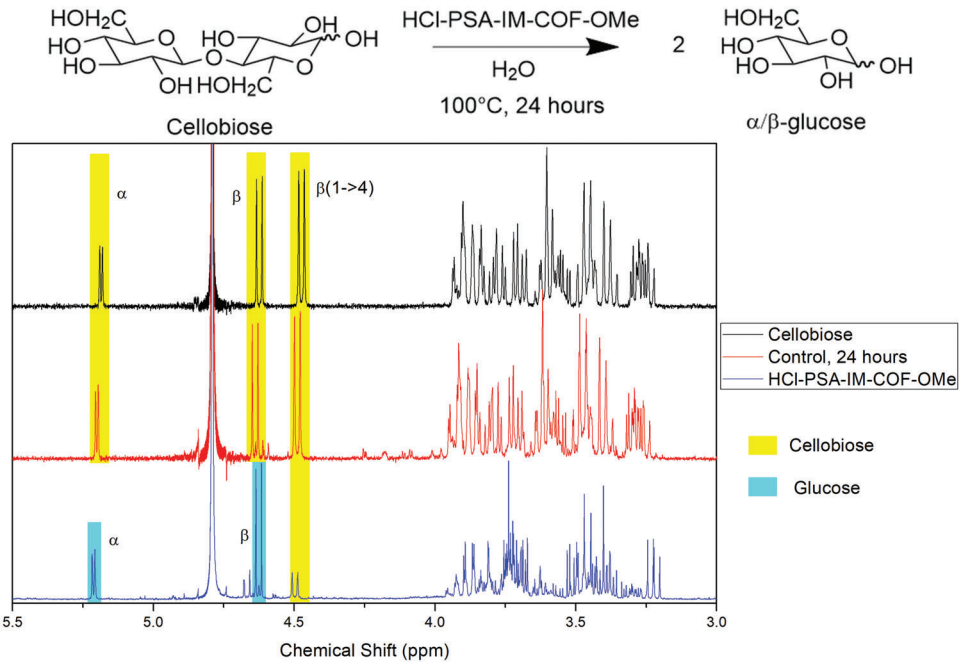

Figure 3. Hydrolysis of cellobiose in the presence of HCl-PSA-IM-COF-OMe in neutral aqueous condition at 100 °C. Reaction condition: 25 mg HCl-PSA-IM-COF-OMe, 4 mmol disaccharide per mmol $-SO_3H$, 1 mL deuterium oxide, 100 °C, 24 h. Typical ^{1}HNMR spectra analyses of cellobiose hydrolysis.

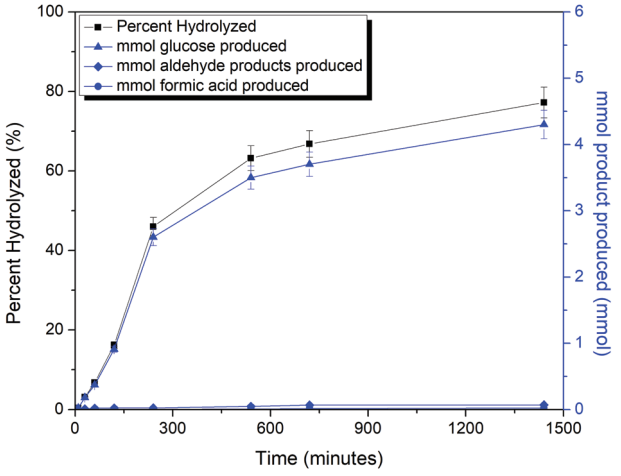

Figure 4. Percent of cellobiose hydrolyzed and amount of glucose, aldehyde derivatives, and formic acid formed versus time. Reaction condition: 50 mg HCl-PSA-IM-COF-OMe, 100 mmol cellobiose per mmol $-SO_3H$, 2 mL deuterium oxide, 100 °C, varied intervals.

Table 1. A summary of control experiments for the hydrolysis of cellobiose.

Catalyst	Percent hydrolyzed (by quantitative ^{1}HNMR)
No COF	1.8
COF-OMe	1.1
IM-COF-OMe	3.3
80 wt% 3-hydroxypropanesulfonic acid (aq)	61.1
IM-COF-OMe and 80 wt% 3-hydroxypropanesulfonic acid (aq)	3.5
Amberlyst 15[a)]	9.8
$[O\text{-PSA}]_{1/3}$-COF-OMe	24.4
PS@HCl-PSA-IM-COF-OMe	37.8

[a)] Amberlyst 15 (4.6 mmol $-SO_3H$ g^{-1}, 36 m^2 g^{-1}), 15.5% hydrolyzed with Lactose. Reaction condition: Catalyst containing 0.0392 mmol $-SO_3H$ equivalent, 40 mmol cellobiose per mmol $-SO_3H$, 1 mL deuterium oxide, 100 °C, 24 h.

Amberlyst 15, however, underperformed at 9.8% conversion, likely due to low surface area which decreases accessibility of sulfonic acid groups. Other common disaccharides were also tested in the same condition and are summarized in **Table 2**.

2.3. Importance of the Ionic Moiety

The boost in hydrolysis can be best explained by the spatial isolation of all hydrolytic components within the pore environment—the donation of protons from the dangling propyl sulfonic acid groups to the oxygen of glycosidic bonds, oxocarbenium ion formation and stabilization by pore chloride ion,[25] subsequent nucleophilic attack with water, and proton transfer to either back to sulfonic acid or to water to restart the catalytic cycle. To illustrate the importance of the imidazolium chloride moiety, an acidic control COF, $[O\text{-PSA}]_{1/3}$-COF-OMe in which one third of DMTP monomers were substituted with dihydroxyterephthaldehyde (DHTP) and subsequently functionalized with propyl sulfonic acid at the hydroxy position, was synthesized (structure shown in Figure S12, Supporting Information). The sulfur content of $[O\text{-PSA}]_{1/3}$-COF-OMe was determined to be 4.24% by elemental analysis and sulfonic acid content 1.1 mmol $-SO_3H$ per gram by titration (Table S1, Supporting Information). When

Table 2. A summary of common disaccharide hydrolysis in the presence of HCl-PSA-IM-COF-OMe. Reaction condition: 25 mg HCl-PSA-IM-COF-OMe, 4 mmol disaccharide per mmol $-SO_3H$, 1 mL deuterium oxide, 100 °C, 24 h.

Disaccharide	Products	Linkage	ΔG° [kJ mol^{-1}][a)]	Percent hydrolyzed (by quantitative ^{1}HNMR)
α-*p*NPG[b)]	α/β-glucose and *p*NP[c)]	α(1→4)	—[d)]	97.7
β-*p*NPG[b)]	α/β-glucose and *p*NP[c)]	β(1→4)	—[d)]	95.1
Cellobiose	2 α/β-glucose	β(1→4)	−16.0	77.5
Lactose	α/β-galactose and α/β-glucose	β(1→4)	−15.9	94.8
Maltose	2 α/β-glucose	α(1→4)	−15.5	96.1
Sucrose	α/β-glucose and α/β-fructose	α(1→2) β	−26.5	>99.5
Trehalose	2 α/β-glucose	α(1→1) α	−11.8	21.3

[a)] Literature values; [b)] 4-nitrophenyl alpha/beta-D-glucopyranoside; [c)] para-nitrophenol; [d)] No literature value found.

$[O\text{-PSA}]_{1/3}$-COF-OMe was subjected to the same reaction conditions as HCl-PSA-IM-COF-OMe, the percent of cellobiose hydrolyzed was only 24.4%, despite the much, much higher surface area (1868 m^2 g^{-1}) and the higher sulfonic acid content. The pores of HCl-PSA-IM-COF-OMe were also either completely or partially blocked by polymerizing styrene to decrease the accessibility of cellobiose to imidazolium chloride and propyl sulfonic acids (denoted as PS@HCl-PSA-IM-COF-OMe, PS = polystyrene, structure shown in Figure S13, Supporting Information). While both functionalities were still present in the pore, the percent of cellobiose hydrolyzed decreased to 37.8%. Both these control experiments, absence of and decreased accessibility of imidazolium chloride to cellobiose, demonstrated the importance of the ionic moiety to the hydrolysis of cellobiose.

To understand the interaction between the ionic moiety imidazolium chloride and cellobiose, a representative ionic liquid model compound, 1-methyl-3-(3-sulfopropyl)-imidazolium chloride (PSAmim-Cl), was synthesized and their non-covalent interactions were analyzed using NMR. In DMSO-$_{d6}$, the hydroxy hydrogens of cellobiose were well represented on the NMR spectrum (Figure S32, Supporting Information). When small amounts of PSAmim-Cl were added (molar ratio of 1 PSAmim-Cl to 5 cellobioses), the active hydroxy hydrogen peaks merged as one broad peak, indicating multiple interactions between the two molecules. As the molar ratio increased, the merged peak not only became sharper but also shifted downfield toward δ5.98, corresponding to the active proton of sulfonic acid. In parallel, all protons of 1-methyl-3-(3-sulfopropyl)-imidazolium cation also experienced slight chemical shifts as the molar ratio increased (especially when greater than 1:1), meaning the entire cation is participating in this interaction with cellobiose. At higher molar ratio, the imidazolium cation displaced DMSO-$_{d6}$ molecules and became the primary, if not the sole, solvation shell for cellobiose, as predicted by various derivatives of dialkylimidazolium ionic liquid.[26] A similar experiment was performed with cellobiose octaacetate where hydroxyl groups were acetylated, removing its hydrogen bonding donating and accepting abilities. Unsurprisingly, no peaks were merged, broadened, sharpened, nor shifted, indicating no special interactions between PSAmim-Cl and cellobiose octaacetate (Figure S33, Supporting Information). While the extend of this interaction warrants greater interest for cellulose degradation, it is well beyond the scope of current work.

^{35}Cl NMR was attempted to detect weak hydrogen bonding or anionic interactions (Figure S34, Supporting Information), but no useful information can be concluded from their extremely broad peaks (>200 ppm) due to the highly asymmetric nature of the imidazolium chloride-cellobiose complex and due to the quadrupolar nuclei of ^{35}Cl (3/2 spin). Nonetheless, the chloride anions appeared to serve dual roles. According to Remsing et al., chloride anions were mainly responsible for the interaction with cellobiose, with participation from imidazolium cations. Using $^{35/37}$Cl NMR T1/T2 relaxation experiments, Remsing et al. determined the interaction to be a weak hydrogen bond between the chloride anions and the hydroxy groups of cellobiose.[27] Second, the chloride anions were reported to aid in stabilizing the oxocarbenium ion, which is formed during the hydrolysis of glycosidic bonds.[6a,25a,25c] Considering the proximity of all the reactive species in the pores of HCl-PSA-IM-COF-OMe, as well as the results of the two control experiments, this stabilization by chloride anions should lower the energy barrier needed for the formation of oxocarbenium ions, allowing for the addition of water in the subsequent steps in the hydrolysis.

3. Kinetic Studies

To further understand the reaction mechanism in this system, several fundamental kinetic studies were performed. To determine the reaction order, the reaction rates of different molar ratios of cellobiose to sulfonic acid (4:1, 10:1, 40:1, and 100:1) were examined (Table S6, Supporting Information). Comparing the reaction rate k with various molar ratios, the reaction order was determined to be 1 (consistent with homogeneous hydrolysis), meaning the reaction rate was influenced solely by the concentration of cellobiose. With this, a cellobiose conversion of 73.6% was achieved with a 500:1 molar ratio, demonstrating its potential for large scale reactions. Along with reaction rate data at five different temperatures (60, 70, 80, 90, and 100 °C) (Figure S18, Supporting Information), the apparent activation energy of the reaction catalyzed by HCl-PSA-IM-COF-OMe was calculated to be 89.1 kJ mol^{-1} (R^2 = 0.99) in neutral aqueous condition (Figure S19, Supporting Information), which is comparable to the homogeneous sulfuric acid in aqueous γ-valerolactone (at 81.0 kJ mol^{-1}) and 1-ethyl-3-methylimidazolium chloride ([EMIm]Cl) ionic liquid (at 85.0 kJ mol^{-1})[28] but better than the heterogeneous sulfonated co-carbonized β-cyclodextrin

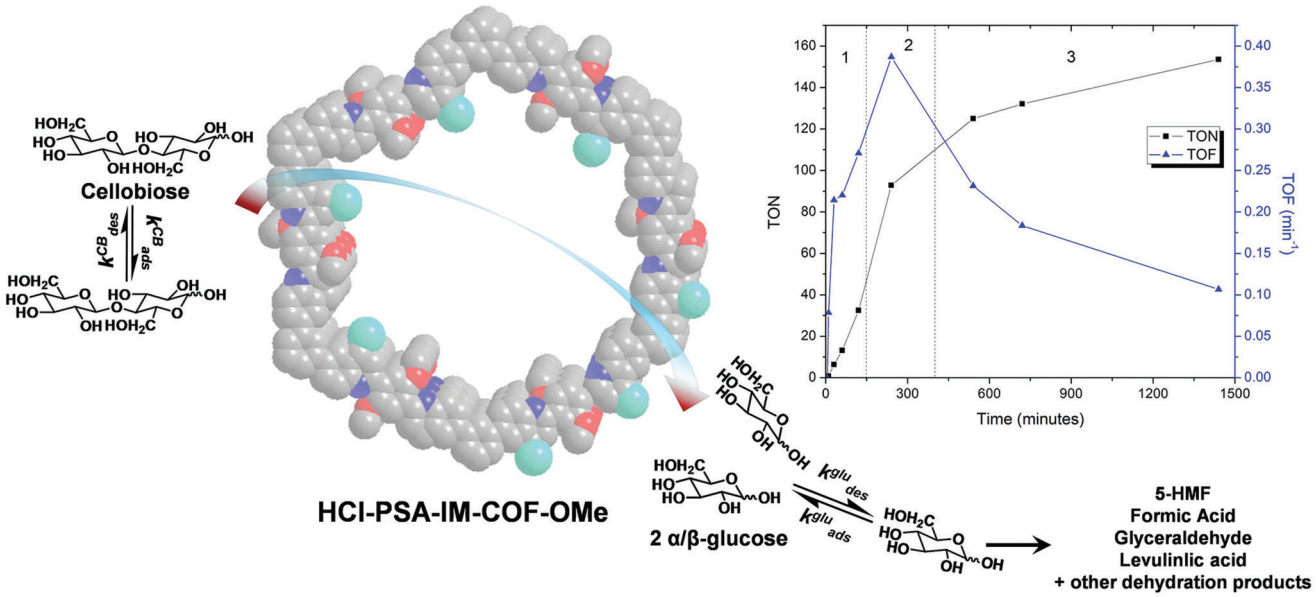

Figure 5. Illustration of the downhill, physiochemical dynamics of cellobiose hydrolysis on the pore surface of HCl-PSA-IM-COF-OMe. Top right—a plot of TON and TOF versus time. The three distinct stages of the hydrolysis: 1) from $t = 0$ to 150 min where $k^{CB}{}_{ads}$, $k^{glu}{}_{des}$, and $k_{hydrolysis}$ are the highest, 2) from $t = 150$ to 360 min where the system transitions from kinetic control to equilibrium control, and 3) from $t = 360$ to 1440 min where the adsorption equilibrium constant, K_{ads}, of cellobiose and glucose comes into full effect, competing for surface interaction with HCl-PSA-IM-COF-OMe.

and poly(vinylchloride) (PVC) in water (at 98.6 kJ mol^{-1})[29] and heterogeneous, heterometallic anionic complexes in 1-butyl-3-methylimidazolium chloride ([BMIm]Cl) (at 95.8 kJ mol^{-1}).[30] The high apparent activation energy is in good agreement with the stability of the glycosidic bonds as well as the temperature sensitivity nature of this reaction. At 90 °C or below, the reaction barely proceeds. Once the energetic barrier is overcome at 100 °C, the reaction rate increased dramatically.

To gain insight into the mechanics of this system, several characteristics of HCl-PSA-IM-COF-OMe and kinetic data were considered. To start, the hydrolysis of cellobiose has a standard Gibbs free energy of −16.0 kJ mol^{-1},[13,31] meaning the glucose products are thermodynamically more stable than cellobiose and are not energetically favorable to condense back to cellobiose. Next, in heterogeneous catalysis, another kinetic consideration is the adsorption and desorption dynamics of cellobiose and glucose to HCl-PSA-IM-COF-OMe.[32] For each molecule, there is an associated rate for the adsorption process and the desorption process ($k^{CB}{}_{ads}$, $k^{CB}{}_{des}$, $k^{glu}{}_{ads}$, $k^{glu}{}_{des}$, where k = rate, CB = cellobiose, glu = glucose, ads = adsorption, des = desorption). At the beginning of the reaction, where all active sulfonic acid sites are open, cellobiose is free to bind with no competition from glucose. However, there is a latency period where cellobioses are binding or are bound but are not hydrolyzed due to the high energetic barrier (89.1 kJ mol^{-1} of apparent activation energy). This latency period is apparent when examining the plot of cellobiose conversion over time, where the percent hydrolyzed is still below 7% 60 min into the reaction (Figure 4). Once the energetic barrier is overcome, the hydrolysis rate increases. Since the concentration of desorbed glucose is low downstream, the rate of glucose desorption increases, increasing the concentration in solution rapidly, as detected by ^{1}HNMR. This phase of the reaction is driven entirely by a downhill kinetics to increase the concentration of desorbed glucose and is not affected by the number of available active sulfonic acid sites, fitting of a first order reaction. As the concentration of desorbed glucose increases in the system, it reaches a maximum rate at about 240 min, as shown in a plot of turnover frequency (TOF) over time (**Figure 5**). At this phase, the system begins the transition from kinetic control to thermodynamic control, as exemplified by the dramatic decrease in TOF. As stated previously, condensation of glucose is disfavored in water. Thus, the dramatic decrease in TOF can only be explained by the adsorption and desorption dynamics of cellobiose and glucose, rather than condensation of glucose. The adsorption equilibrium constants, K_{ads}, for cellobiose (6.75 M^{-1}) and glucose (25.6 M^{-1}) were derived from the linearized form of Langmuir isotherm, and with a significantly higher affinity to HCl-PSA-IM-COF-OMe, glucose adsorption is highly favored at or near equilibrium conditions which competes with the adsorption of cellobiose and its hydrolysis, resulting in the decrease in turnover number (TON) and TOF. This competitive binding, driven by their adsorption equilibrium constants, is especially evident when comparing the cellobiose conversion during the first 12 h (66.8%) and the second 12 h (10.7%).

4. Recyclability and Regeneration

To evaluate the recyclability of this system, HCl-PSA-IM-COF-OMe was filtered, dried, and reused in reactions with lactose and water. As shown in Figure S24a, Supporting Information, the percent conversion decreased gradually after each cycle, down to 59.5% after the fifth cycle. The FTIR spectrum of HCl-PSA-IM-COF-OMe after each cycle (Figure S21, Supporting Information) was measured and found that sulfonic acid groups were preserved. PXRD patterns also showed no loss of crystallinity and BET analyses showed minimal loss in surface area (Figure S20

and Table S8, Supporting Information). The decrease in activity can likely be explained by the residual bound glucose and the gradual proton loss in aqueous medium. As mentioned previously, the binding affinity, K_{ads}, of glucose is quite high and is a favorable, spontaneous process, thus washing in water and tetrahydrofuran may not completely remove all bound glucose. In this catalytic system, the most basic molecule is surprisingly water ($pK_a \approx 15.7$, pK_a of hydronium ≈ -1.7) while the propyl sulfonic acid from the framework is the most acidic ($H_0 \approx 1.64$ and $pK_a \approx -2.6$, based on methanesulfonic acid). Over five catalytic cycles, it is reasonable to assume a portion of the acidic proton will be displaced and, along with occupied acid sites, decreases the overall hydrolytic capability. Knowing this, HCl-PSA-IM-COF-OMe can be regenerated by soaking into diluted hydrochloric acid overnight to restore its hydrolytic ability (back to 86.0% percent conversion, Figure S24b, Supporting Information) while preserving its functional groups, structure, and porosity. The ease of recycling, regenerating its hydrolytic capability, and the first order kinetics of this system make HCl-PSA-IM-COF-OMe a suitable substitute for traditional homogeneous acid catalysts, reducing acidic waste.

5. Conclusions

In this work, we explored the hydrolytic capabilities of an ultrastable quinoline-linked sulfonic acid functionalized COFs on the glycosidic bond of cellobiose and other common disaccharides in neutral, metal-free, and aqueous conditions. Through favorable surface binding interaction to the framework and stabilization of oxocarbenium intermediates, HCl-PSA-IM-COF-OMe provided an ideal reaction environment for the efficient hydrolysis of glycosidic bonds, drastically decreasing the apparent activation energy to 89.1 kJ mol^{-1} by stabilizing the oxocarbenium ion intermediate better than its free molecular acid counterpart and many traditional homogeneous acids in aqueous condition. The dynamic adsorption and desorption behavior of cellobiose and glucose, and their roles in hydrolysis were also investigated. Along with its recyclability and its regeneratability, HCl-PSA-IM-COF-OMe showed a strong potential in large scale hydrolytic applications, where large volumes of acid waste can be reduced by switching to retrievable solid acid catalysts. This approach to incorporate multiple specific, non-covalent interactions around a catalytic center in a confined pore environment is highly reminiscent to biological systems and is relevant for the development of next generation heterogeneous catalysts.

6. Experimental Section

Chemicals: Solvents were purified according to standard laboratory methods. Other commercially available reagents were purchased in high purity and used without further purification.

Monomer Syntheses: 1,3,5-tris(4-aminophenyl)benzene (TAPB), 2,5-dimethoxyterephthalaldehyde (DMTP), and 2,5-dihydroxyterephthalaldehyde (DHTP) were synthesized according to previously reported methods.[1a]

Synthesis of COF-OMe: In a 50 mL Schlenk tube, 422 mg (1.20 mmol) of 1,3,5-tris(4-aminophenyl)benzene and 350 mg of 2,5-dimethoxyterephthalaldehyde (1.80 mmol) were added, followed by 16.5 mL of 5:5:1 v/v/v solution of 1,2-dichlorobenzene/*n*-butanol/6 M aqueous acetic acid. After sonication, the tube was flash frozen at 77 K in a liquid nitrogen bath, evacuated, and sealed. Once at room temperature, it was heated at 120 °C for 72 h to afford a bright yellow solid which was collected by vacuum filtration and washed with tetrahydrofuran in a Soxhlet extractor for 24 h. Afterward, the solid was dried at 100 °C for subsequent use.

Synthesis of IM-COF-OMe: In a one pot synthesis, dried COF-OMe (600 mg), $Yb(OTf)_3$ (300 mg, 0.48 mmol), DDQ (300 mg, 1.125 mmol), 1-vinylimidazole (5 mL, 55.2 mmol), and 100 mL anhydrous acetonitrile were heated at reflux for 72 h under Argon atmosphere to afford a red–orange solid which was collected by vacuum filtration and washed with tetrahydrofuran in a Soxhlet extractor for 24 h. Afterward, the solid was dried at 100 °C for subsequent use.

Synthesis of HCl-PSA-IM-COF-OMe: In a one pot synthesis, dried IM-COF-OMe (500 mg), 1,3-propane sultone (500 mg, 4.95 mmol), and 75 mL of anhydrous toluene were heated at reflux for 24 h under Argon atmosphere.[21a] Once cooled to room temperature, 0.05 mM aqueous hydrochloric acid was added and stirred for 1 h. The deep red solid was then collected by vacuum filtration and washed with tetrahydrofuran in a Soxhlet extractor for 24 h. Afterward, the solid was dried at 100 °C for subsequent use.

Synthesis of [O-PSA]$_{1/3}$-COF-OMe: In a 50 mL Schlenk tube, 422 mg (1.20 mmol) of 1,3,5-tris(4-aminophenyl)benzene, 233 mg of 2,5-dimethoxyterephthalaldehyde (1.20 mmol), and 100 mg of 2,5-dihydroxyterephthalaldehyde (0.60 mmol) were added, followed by 16.5 mL of 5:5:1 v/v/v solution of 1,2-dichlorobenzene/*n*-butanol/6 M aqueous acetic acid. After sonication, the tube was flash frozen at 77 K in a liquid nitrogen bath, evacuated, and sealed. Once at room temperature, it was heated at 120 °C for 72 h to afford a bright yellow solid which was collected by vacuum filtration and washed with tetrahydrofuran in a Soxhlet extractor for 24 h. Afterward, the solid was dried at 100 °C for subsequent use. In a one pot synthesis, dried [OH]$_{1/3}$-COF-OMe (500 mg), 1,3-propane sultone (500 mg, 4.95 mmol), and 75 mL of anhydrous toluene were heated at reflux for 24 h under Argon atmosphere. The deep red solid was then collected by vacuum filtration and washed with tetrahydrofuran in a Soxhlet extractor for 24 h. Afterward, the solid was dried at 100 °C for subsequent use.

Synthesis of PS@HCl-PSA-IM-COF-OMe: In a one pot synthesis, dried HCl-PSA-IM-COF-OMe (500 mg), styrene (500 mg, 4.80 mmol), azobisisobutyronitrile (AIBN, 10.0 mg), and 20 mL of anhydrous DMF were stirred for 24 h under Argon atmosphere. Afterward, the mixture was heated at 80 °C for 3 days, which was then collected by vacuum filtration and washed with DMF and tetrahydrofuran. The orange solid was dried at 100 °C for subsequent use.

Synthesis of 1-Methyl-3-(3-sulfopropyl)-imidazolium chloride (PSAmim-Cl): Equimolar (10 mmol) of 1-methylimidazole and 1,3-propane sultone were dissolved in 30 mL of anhydrous toluene. It was then refluxed in argon atmosphere for 24 h under stirring. The product was precipitated as a white solid and was isolated by filtration, washed with additional toluene, and dried at 80 °C for 6 h. Equimolar of this dried white solid and 37 wt% hydrochloric acid were mixed and heated at 90 °C for 24 h to yield PSAmim-Cl as viscous yellow oil after separation from water. ^{1}H NMR (400 MHz, DMSO-d_6, δ) 9.16 (s, 1H, Ar-H), 7.76 (t, J = 1.8 Hz, 1H, Ar–H), 7.69 (t, J = 1.7 Hz, 1H, Ar–H), 5.96 (s, 6H, –SO_3H), 4.25 (t, J = 7.0 Hz, 2H, N$^+$–CH_2–), 3.81 (s, 3H, –CH_3), 2.46 (t, 2H, –CH_2–S), 2.05 (qu, 2H, C–CH_2–C).

Fourier Transform Infrared Spectroscopy: FTIR spectra were measured using PerkinElmer UATR Two—Spectrum Two, from 4000 to 500 cm^{-1}.

Brunauer–Emmett–Teller Surface Area Measurement: Using micromeritics 3FLEX, the N_2 gas adsorption isotherms were measured at 77 K in a liquid N_2 bath.

Powder X-Ray Diffraction: PXRD data were collected using Rigaku Ultima III XRD (40 kV and 40 mA) using Cu K_α (λ = 1.5406 Å) radiation.

Sulfonic Acid Content: Back titration with 10 mM $NaOH_{(aq)}$ and 2 M $NaCl_{(aq)}$. The COF sample was soaked in 20 mL 2 M $NaCl_{(aq)}$ solution and subjected to sonication for 2 h. Afterward, the sample was centrifuged at 5000 rpm for 15 min and the entire sample was titrated with 10 mM $NaOH_{(aq)}$ using phenolphthalein as indicator. The total sulfonic acid content was determined using a stoichiometric ratio of 1:1.

Saccharide Uptake—Binding Affinity: 25 mg of HCl-PSA-IM-COF-OMe were soaked in 1 mL of aqueous saccharide solution at various concentrations for 2 h. Afterward, 0.1 mL of 0.4 M maleic acid was added and then the sample was centrifuged. The ^{1}HNMR was acquired and the integrations of the essential peaks were compared to a control without COF addition to determine the amount of saccharide adsorbed by HCl-PSA-IM-COF-OMe. The following equation was used to determine the adsorption equilibrium constant, K_{ads}:

$$\frac{1}{Q_e} = \frac{1}{K_{ads} Q_m c_e} + \frac{1}{Q_m} \quad (1)$$

Saccharide Uptake—PXRD and BET: 25 mg of HCl-PSA-IM-COF-OMe were soaked in 1 mL of 0.2 M aqueous saccharide solution for 2 h. The sample was then filtered and washed in small amounts of tetrahydrofuran to remove excess water. After drying, PXRD and BET surface area of sample were measured.

Elemental Analysis: Samples were sent to Atlantic Microlab.

Water Contact Angle: Approximately 60 mg of COF powder were hydraulically pressed into a disc with an approximate diameter of 12 mm and a height of 0.5 mm. The water contact angle was measured with a 5 µL drop and images were captured using a high-resolution camera and ImageJ Software.

X-Ray Photoelectron Spectroscopy: XPS spectra were performed on a PHI 5000 Versaprobe Scanning XPS Microprobe with Al Kα irradiation at $\theta = 90°$ for X-ray sources, and the binding energies were calibrated using the C 1s peak at 284.9 eV.

Thermogravimetric Analysis: TGA was performed on Thermal Analysis Instruments Q50 at 10.00 °C per minute ramp rate from room temperature up to 800 °C.

^{1}HNMR and ^{13}C and ^{31}P ssNMR: NMR spectra were recorded on Varian 400 and 500 MHz spectrometers.[33]

Scanning Electron Microscopy: SEM images were captured using FEI Nova NanoSEM 230.

Hammett Acidity Function: H_0 values were determined using 4-nitroaniline (5 mg L^{-1}) as the probe molecule and sulfonic acids (25 mmol $-SO_3H$ L^{-1}) in aqueous conditions. After soaking for 24 h at room temperature, UV–vis spectrum was measured from 300 to 500 nm. Max absorbance at 380 nm was used for the calculation of Hammett Relative Acidity Function using the following equation:

$$H_0 = pK(I)_{aq} + \log \frac{[I]}{[IH^+]} \quad (2)$$

Where $pK(I)_{aq}$ is the pK_a value of the 4-nitroaniline indicator solution, which is 0.99; [I] and [IH^+] are the molar concentrations of the protonated and unprotonated forms of 4-nitroaniline indicator, respectively.

NMR Studies of PSAmim-Cl and Cellobiose Interactions: In an NMR tube, 0.005 g (0.02 mmol) of PSAmim-Cl and 0.035 g (0.1 mmol) of cellobiose were dissolved in 0.75 mL of DMSO-$_{d6}$. ^{1}HNMR spectrum was acquired with standard parameters at 128 scans. Spectra of increasing PSAmim-Cl were acquired in a similar way. For cellobiose octaacetate, 0.005 g (0.02 mmol) of PSAmim-Cl and 0.068 g (0.1 mmol) of cellobiose octaacetate were used instead.

Cellobiose Hydrolysis: In a typical reaction, 25 mg of HCl-PSA-IM-COF-OMe (0.56 mmol $-SO_3H$ per gram COF), 0.1920 g cellobiose (0.561 mmol, 40 glycosidic bonds:1 $-SO_3H$ site), and 1 mL of deuterium oxide were added together in a 10 mL glass vial with a stir bar. The mixture was heated at 100 °C for 24 h in an oil bath. To analyze the product, the mixture was cooled, 0.025 mL of 0.4 M of maleic acid was added, and then centrifuged to separate the COF. The ^{1}HNMR spectrum was taken and, using the maleic acid as internal reference, the yield of glucose and any of its derivatives were calculated.

Common Disaccharide Hydrolysis: Same as cellobiose hydrolysis, except cellobiose was substituted with common disaccharides at same essential glycosidic bond concentrations.

Reference Materials: Same as cellobiose hydrolysis, except HCl-PSA-IM-COF-OMe was substituted with reference materials at the same $-SO_3H$ concentration. For materials without $-SO_3H$ groups, the same mass was used instead.

Recycling Test: After reaction, the COF was recycled by first filtration from reaction medium, followed by washing with water and tetrahydrofuran in a Soxhlet extractor for 24 h. After drying, the COF was ready for use for subsequent use.

Regeneration of HCl-PSA-IM-COF-OMe: The spent COF catalyst can be regenerated by soaking in 0.05 mM aqueous hydrochloric acid for 12 h. It was then filtered and washed with tetrahydrofuran in a Soxhlet extractor for 24 h. Afterward, the solid was dried at 100 °C for subsequent use.

Reaction Rate: To determine the reaction rate, multiple reactions were set up and stopped at indicated time intervals (5, 10, 30, 60, 120, 240, 540, 720, 1440, and 1560 min). Once cooled, 0.025 mL of 0.4 M maleic acid$_{(aq)}$ was added, centrifuged, and the ^{1}HNMR spectrum was taken using maleic acid as internal reference. The reaction rate was determined using the following equations:

$$-\frac{d[\text{cellobiose}]}{dt} = k[\text{cellobiose}] \quad (3)$$

$$\ln[\text{cellobiose}]_0 - \ln[\text{cellobiose}]_t = kt \quad (4)$$

Reaction Order: Various cellobiose to $-SO_3H$ molar ratios (4:1, 10:1, 40:1, and 100:1) were used to determine the reaction order. Typically, 25 mg of HCl-PSA-IM-COF-OMe, cellobiose at different molar ratios, 1 mL water, and 100 °C were used. The reactions were stopped at 6 h to maintain a less than 100% conversion for accurate reaction order determination.

Apparent Activation Energy Determination: The reaction rate determination experiments were repeated at different temperatures (60, 70, 80, 90, and 100 °C). 25 mg of HCl-PSA-IM-COF-OMe, 0.1920 g of cellobiose, and 1 mL of deuterium oxide were used. For optimal results, times with less than 20% conversion were used in the calculation of apparent activation energy, using the following equation:

$$\ln k = -\frac{E_a}{RT} + \ln A \quad (5)$$

Supporting Information

Supporting Information is available from the Wiley Online Library or from the author.

Acknowledgements

The authors acknowledge the Robert A. Welch Foundation (No. B-0027) for financial support of this work.

Conflict of Interest

The authors declare no conflict of interest.

Data Availability Statement

The data that support the findings of this study are available from the corresponding author upon reasonable request.

Keywords

covalent organic frameworks, enzyme mimicries, general acid catalyses, glycosidic bonds, heterogeneous catalysts, non-covalent interactions, quinoline-linked polymers

Received: September 2, 2022
Revised: October 31, 2022
Published online: November 23, 2022

[1] a) Q. Sun, Y. Tang, B. Aguila, S. Wang, F. S. Xiao, P. K. Thallapally, A. M. Al-Enizi, A. Nafady, S. Ma, *Angew. Chem., Int. Ed. Engl.* **2019**, *58*, 8670; b) S. A. Cook, A. S. Borovik, *Acc. Chem. Res.* **2015**, *48*, 2407; c) M. Raynal, P. Ballester, A. Vidal-Ferran, P. W. van Leeuwen, *Chem. Soc. Rev.* **2014**, *43*, 1734; d) G. Yang, X. Luo, L. Shuai, *Front. Bioeng. Biotechnol.* **2021**, *9*, 770027.

[2] a) A. J. Neel, M. J. Hilton, M. S. Sigman, F. D. Toste, *Nature* **2017**, *543*, 637; b) F. D. Toste, M. S. Sigman, S. J. Miller, *Acc. Chem. Res.* **2017**, *50*, 609; c) L. Liu, T. Y. Zhou, S. G. Telfer, *J. Am. Chem. Soc.* **2017**, *139*, 13936; d) M. Zhao, K. Yuan, Y. Wang, G. Li, J. Guo, L. Gu, W. Hu, H. Zhao, Z. Tang, *Nature* **2016**, *539*, 76.

[3] a) Y. Sakamoto, K. Imamura, A. Onda, *ACS Omega* **2020**, *5*, 24964; b) J. Meeuwissen, J. N. Reek, *Nat. Chem.* **2010**, *2*, 615; c) N. A. Grosso-Giordano, C. Schroeder, A. Okrut, A. Solovyov, C. Schottle, W. Chasse, N. Marinkovic, H. Koller, S. I. Zones, A. Katz, *J. Am. Chem. Soc.* **2018**, *140*, 4956.

[4] a) J. Guo, D. Jiang, *ACS Cent. Sci.* **2020**, *6*, 869; b) X. Zhao, P. Pachfule, S. Li, T. Langenhahn, M. Ye, C. Schlesiger, S. Praetz, J. Schmidt, A. Thomas, *J. Am. Chem. Soc.* **2019**, *141*, 6623.

[5] a) D. Yamaguchi, K. Watanabe, S. Fukumi, *Sci. Rep.* **2016**, *6*, 20327; b) F. Yang, Y. Li, Q. Zhang, X. Sun, H. Fan, N. Xu, G. Li, *Carbohydr. Polym.* **2015**, *131*, 9.

[6] a) C. Loerbroks, R. Rinaldi, W. Thiel, *Chemistry* **2013**, *19*, 16282; b) P. Chen, A. Shrotri, A. Fukuoka, *Catal. Sci. Technol.* **2020**, *10*, 4593.

[7] a) T. J. Tse, D. J. Wiens, M. J. T. Reaney, *Fermentation* **2021**, *7*, 268; b) N. S. Mat Aron, K. S. Khoo, K. W. Chew, P. L. Show, W. H. Chen, T. H. P. Nguyen, *Int. J. Energy Res.* **2020**, *44*, 9266.

[8] a) K. Robak, M. Balcerek, *Food Technol. Biotechnol.* **2018**, *56*, 174; b) H. K. Noh, S.-Y. No, *Appl. Energy* **2017**, *208*, 782.

[9] a) S. Zhong, R. Daniel, H. Xu, J. Zhang, D. Turner, M. L. Wyszynski, P. Richards, *Energy Fuels* **2010**, *24*, 2891; b) J. Frost, P. Hellier, N. Ladommatos, *Fuel* **2021**, *313*, 122663; c) A. T. Hoang, S. Nizetic, V. V. Pham, *Environ. Sci. Pollut. Res.* **2021**, *28*, 4918; d) H. Liu, X. Wang, D. Zhang, F. Dong, X. Liu, Y. Yang, H. Huang, Y. Wang, Q. Wang, Z. Zheng, *Energies* **2019**, *12*, 1845; e) K. Alexandrino, *Energy Fuels* **2020**, *34*, 6598; f) T. T. Bui, D. Balasubramanian, A. T. Hoang, O. Konur, D. C. Nguyen, V. N. Tran, *Energy Sources, Part A: Recovery, Utilization, and Environmental Effects*, **2020**, 1. https://doi.org/10.1080/15567036.2020.1869868

[10] F. Y. Yan, W. Xia, X. X. Zhang, S. Chen, X. Z. Nie, L. C. Qian, *J. Zhejiang Univ., Sci., B* **2016**, *17*, 455.

[11] a) M. Marzo, A. Gervasini, P. Carniti, *Carbohydr. Res.* **2012**, *347*, 23; b) K. Cho, S. M. Lee, H. J. Kim, Y. J. Ko, S. U. Son, *Chem. Commun.* **2019**, *55*, 3697; c) R. Rinaldi, R. Palkovits, F. Schuth, *Angew. Chem., Int. Ed. Engl.* **2008**, *47*, 8047.

[12] a) B. C. Knott, M. H. Momeni, M. F. Crowley, L. F. Mackenzie, A. W. Gotz, M. Sandgren, S. G. Withers, J. Stahlberg, G. T. Beckham, *J. Am. Chem. Soc.* **2014**, *136*, 321; b) I. V. Khavrutskii, J. R. Compton, K. M. Jurkouich, P. M. Legler, *Biochemistry* **2019**, *58*, 5351; c) J. E. Nielsen, J. A. McCammon, *Protein Sci.* **2003**, *12*, 1894.

[13] T. H. Sorensen, N. Cruys-Bagger, K. Borch, P. Westh, *J. Biol. Chem.* **2015**, *290*, 22203.

[14] a) J. Ma, T. Li, H. Tan, W. Liu, H. Yin, *Front. Mol. Biosci.* **2020**, *7*, 569797; b) X. Zhang, S. Wang, X. Wu, S. Liu, D. Li, H. Xu, P. Gao, G. Chen, L. Wang, *Sci. Rep.* **2015**, *5*, 18357.

[15] a) V. Spiwok, *Molecules* **2017**, *22*, 1038; b) W. Chen, S. Enck, J. L. Price, D. L. Powers, E. T. Powers, C. H. Wong, H. J. Dyson, J. W. Kelly, *J. Am. Chem. Soc.* **2013**, *135*, 9877.

[16] C. Wang, K. Liao, *ACS Appl. Mater. Interfaces* **2021**, *13*, 56752.

[17] a) A. P. Cote, A. I. Benin, N. W. Ockwig, M. O'Keeffe, A. J. Matzger, O. M. Yaghi, *Science* **2005**, *310*, 1166; b) S. Kandambeth, K. Dey, R. Banerjee, *J. Am. Chem. Soc.* **2019**, *141*, 1807; c) R. P. Bisbey, W. R. Dichtel, *ACS Cent. Sci.* **2017**, *3*, 533; d) Y. Song, Q. Sun, B. Aguila, S. Ma, *Adv. Sci.* **2019**, *6*, 1801410; e) F. Beuerle, B. Gole, *Angew. Chem., Int. Ed. Engl.* **2018**, *57*, 4850.

[18] a) Q. Sun, C. W. Fu, B. Aguila, J. Perman, S. Wang, H. Y. Huang, F. S. Xiao, S. Ma, *J. Am. Chem. Soc.* **2018**, *140*, 984; b) C. R. Mulzer, L. Shen, R. P. Bisbey, J. R. McKone, N. Zhang, H. D. Abruna, W. R. Dichtel, *ACS Cent. Sci.* **2016**, *2*, 667; c) H. Ma, B. Liu, B. Li, L. Zhang, Y. G. Li, H. Q. Tan, H. Y. Zang, G. Zhu, *J. Am. Chem. Soc.* **2016**, *138*, 5897; d) Q. Sun, Y. Pan, X. Wang, H. Li, J. Farmakes, B. Aguila, Z. Yang, S. Ma, *Chem* **2019**, *5*, 3184.

[19] a) J. Jiang, O. M. Yaghi, *Chem. Rev.* **2015**, *115*, 6966; b) Y. Peng, Z. Hu, Y. Gao, D. Yuan, Z. Kang, Y. Qian, N. Yan, D. Zhao, *ChemSusChem* **2015**, *8*, 3208; c) Q. Sun, B. Aguila, L. D. Earl, C. W. Abney, L. Wojtas, P. K. Thallapally, S. Ma, *Adv. Mater.* **2018**, *30*, 1705479; d) N. Huang, X. Chen, R. Krishna, D. Jiang, *Angew. Chem., Int. Ed. Engl.* **2015**, *54*, 2986.

[20] a) Y. Pramudya, J. L. Mendoza-Cortes, *J. Am. Chem. Soc.* **2016**, *138*, 15204; b) M. S. Lohse, T. Stassin, G. Naudin, S. Wuttke, R. Ameloot, D. De Vos, D. D. Medina, T. Bein, *Chem. Mater.* **2016**, *28*, 626; c) A. Nagai, Z. Guo, X. Feng, S. Jin, X. Chen, X. Ding, D. Jiang, *Nat. Commun.* **2011**, *2*, 536.

[21] a) B. J. Yao, W. X. Wu, L. G. Ding, Y. B. Dong, *J. Org. Chem.* **2021**, *86*, 3024; b) A. S. Amarasekara, O. S. Owereh, *Catal. Commun.* **2010**, *11*, 1072; c) X. Li, C. Zhang, S. Cai, X. Lei, V. Altoe, F. Hong, J. J. Urban, J. Ciston, E. M. Chan, Y. Liu, *Nat. Commun.* **2018**, *9*, 2998; d) X. T. Li, J. Zou, T. H. Wang, H. C. Ma, G. J. Chen, Y. B. Dong, *J. Am. Chem. Soc.* **2020**, *142*, 6521; e) C. Li, Y. Ma, H. Liu, L. Tao, Y. Ren, X. Chen, H. Li, Q. Yang, *Chin. J. Catal.* **2020**, *41*, 1288.

[22] D. J. Dibble, M. J. Umerani, A. Mazaheripour, Y. S. Park, J. W. Ziller, A. A. Gorodetsky, *Macromolecules* **2015**, *48*, 557.

[23] a) C. E. Hernandez-Tamargo, A. Roldan, N. H. de Leeuw, *J. Phys. Chem. C* **2016**, *120*, 19097; b) C. Bornes, M. Sardo, Z. Lin, J. Amelse, A. Fernandes, M. F. Ribeiro, C. Geraldes, J. Rocha, L. Mafra, *Chem. Commun.* **2019**, *55*, 12635; c) E. Pires, J. M. Fraile, *Phys. Chem. Chem. Phys.* **2020**, *22*, 24351.

[24] a) K. Selvam, D. Senbagam, T. Selvankumar, C. Sudhakar, S. Kamala-Kannan, B. Senthilkumar, M. Govarthanan, *J. Mol. Struct.* **2017**, *1150*, 61; b) S. Arola, M. B. Linder, *Sci. Rep.* **2016**, *6*, 35358; c) M. Paul, G. Panda, P. K. D. Mohapatra, H. Thatoi, *J. Mol. Struct.* **2020**, *1204*, 127547.

[25] a) M. A. Mellmer, C. Sanpitakseree, B. Demir, K. Ma, W. A. Elliott, P. Bai, R. L. Johnson, T. W. Walker, B. H. Shanks, R. M. Rioux, M. Neurock, J. A. Dumesic, *Nat. Commun.* **2019**, *10*, 1132; b) T. Yang, Y. Sun, H. Wang, Z. Lin, J. Wen, X. Zhang, *Angew. Chem., Int. Ed. Engl.* **2020**, *59*, 6108; c) T. Qi, Z. B. Si, L. J. Liu, H. M. Yang, Z. Huang, H. Q. Yang, C. W. Hu, *Phys. Chem. Chem. Phys.* **2020**, *22*, 9349.

[26] a) G. H. Richard, C. Remsing, R. P. Swatloski, W. W. Massefski, R. D. Rogers, G. Moyna, *J. Phys. Chem. B* **2008**, *112*, 11071; b) Y. Fukaya, K. Hayashi, M. Wada, H. Ohno, *Green Chem.* **2008**, *10*, 44; c) H. Ohno, Y. Fukaya, *Chem. Lett.* **2009**, *38*, 2.

[27] R. C. Remsing, R. P. Swatloski, R. D. Rogers, G. Moyna, *Chem. Commun.* **2006**, 1271.

[28] M. A. Mellmer, D. M. Alonso, J. S. Luterbacher, J. M. R. Gallo, J. A. Dumesic, *Green Chem.* **2014**, *16*, 4659.

[29] C. Sun, Q. Liao, A. Xia, C. Chen, Q. Fu, Y. Huang, X. Zhu, F. Sun, *Fuel* **2021**, *300*, 120978.

[30] Y. Yang, H. Qi, H. Li, Z. Xu, X. Liu, S. Yu, Z. C. Zhang, *ACS Catal.* **2021**, *11*, 11774.

[31] Y. B. Tewari, B. E. Lang, S. R. Decker, R. N. Goldberg, *J. Chem. Thermodyn.* **2008**, *40*, 1517.

[32] a) M. A. Ardagh, O. A. Abdelrahman, P. J. Dauenhauer, *ACS Catal.* **2019**, *9*, 6929; b) G. Zakem, I. Ro, J. Finzel, P. Christopher, *J. Catal.* **2021**, *404*, 883; c) G. B. Marin, V. V. Galvita, G. S. Yablonsky, *J. Catal.* **2021**, *404*, 745.

[33] a) Q. Sun, K. Hu, K. Leng, X. Yi, B. Aguila, Y. Sun, A. Zheng, X. Meng, S. Ma, F.-S. Xiao, *J. Mater. Chem. A* **2018**, *6*, 18712; b) X. Yi, H. H. Ko, F. Deng, S. B. Liu, A. Zheng, *Nat. Protoc.* **2020**, *15*, 3527.